Plasma carburising for improvement of Ni-Fe cathodes for alkaline water electrolysis

I. Flis-Kabulska[a,b,*], Y. Sun[c], T. Zakroczymski[a], J. Flis[a]

[a] *Institute of Physical Chemistry PAS, Kasprzaka 44/52, 01-224 Warszawa, Poland*

[b] *University of Cardinal Stefan Wyszynski, Wóycickiego 1/3, 01-938 Warszawa, Poland*

[c] *De Montfort University, Leicester LE1 9BH, UK*

ABSTRACT

Electrodeposited Ni-Fe-C alloys have high electroactivity for hydrogen evolution reaction (HER) in alkaline water electrolysis. In the present work carbon was introduced into Ni and Ni–Fe alloys by plasma treatment in CH_4+H_2 gas mixture at 470 °C. Despite of a very low solubility of carbon in nickel, carbon entered into nickel to the depth of about 0.5 μm, formed about 2-μm thick carbide layer in high-Fe alloys, and increased hardness. Electrochemical measurements in 25 wt.% KOH at 80 °C showed that carburization resulted in an improvement of catalytic activity toward HER, especially of Ni and 1Ni-Fe. Carburization also increased the resistance to corrosion during cathodic polarisation and under open-circuit conditions. XPS surface analysis showed that after corrosion the oxide content was on carburized materials significantly lower than that on untreated materials. It is suggested that the enhanced electroactivity of plasma carburized cathodes is due mainly to the enlargement of the surface area of disintegrated material. A catalytic affect might also be exerted by carbon-metal particles.

Keywords: Water electrolysis. Ni-Fe cathodes. Plasma carburizing.

---

* Corresponding author; e-mail ifliskabulska@ichf.edu.pl (I Flis-Kabulska).

1. Introduction

At present the production of hydrogen by water electrolysis is much more expensive than the conversion of natural gas or coal, however, its cost will be decreasing with the increasing availability of renewable energy sources. Electrolysis provides pure hydrogen which is needed to fuel cells for vehicles; it can be conducted also in small-scale installations for use at filling stations. Recent surveys on various technologies of water electrolysis (alkaline, PEM, high-temperature) are presented in [1,2,3,4].

Challenges for further development of alkaline water electrolysis include an improvement of cathodes made from cheap materials. The most widely used are cathodes of nickel and its alloys with Mo and, to a lesser extent, with Fe, W, Ti, Co, V, Cr, Zn [5,6].

Out of these alloying metals, Fe can be the most advantageous owing to its low price and a good electrocatalytic activity for the hydrogen evolution reaction (HER) [4]. Alloys of Ni

with Fe have a better electrocatalytic activity than each of the components alone; this was shown for the alloys obtained both by electrodeposition [7,8,9] and metallurgically [10].

The presence of carbon in electrodeposited alloys strongly enhances their activity. Electrodeposited nanocrystalline Ni-Fe-C alloys showed the highest activity among known electrodes for hydrogen evolution in a hot concentrated alkaline solution [7]. Activity of electrodeposited Ni-Fe-C alloys in seawater electrolysis varies with the grain size [11] and carbon content [12].

Beneficial effect of carbon on activity toward HER was also observed on nickel subjected to low-temperature (470 °C) plasma carburising [13]. This effect was due mainly to carbon which entered into the metal matrix, and less by carbon which was deposited on the surface.

In addition to the enhancement of electrocatalytic activity, low-temperature plasma carburising can increase hardness and corrosion resistance, as observed for austenitic stainless steels [14]. It can be expected that owing to high hardness, plasma carburized cathodes might be more resistant to damaging effect of evolving hydrogen gas, and to corrosion which occurs on hydrogenated nickel alloys [15] and on nickel, iron and Ni-Fe alloys [10].

Solubility of carbon in nickel is very low [16], nevertheless, thin surface films of nickel-carbon can be obtained by high-energy treatments such as plasma alloying [13] or d.c. magnetron sputter deposition [17,18]. An addition of Fe to Ni facilitates uptake of carbon. In a $CO–H_2–H_2O–Ar$ gas at 650 °C, no carbide appeared on Fe-Ni alloys with Ni above 10 wt.%, but carbide Fe_3C layer formed at the surface of Fe, Fe-5Ni and 10Ni-Fe [19].

The aim of the present work was to determine the effect of low-temperature plasma carburizing on hydrogen evolution and on corrosion of Ni-Fe cathodes (wt.% Ni: 90, 60, 10, 1) in hot alkaline solution. It was expected that carburizing will increase both the electroactivity and the resistance to distortion during electrolysis and during corrosion upon switching off the electrolysis.

2. Experimental

Measurements were performed on Ni and Ni-Fe alloys presented in Table 1. Cold rolled rods were machined into samples in form of 2-mm thick discs of 8-mm dia. The samples were ground with a SiC wheel and finally with wet SiC grinding papers up to the 1200 grade.

Carbon was introduced into surface layers in a commercial plasma treatment unit. The process of carburizing was carried out under conditions established in [20]. First, heating of the samples was achieved by ion bombardment in a hydrogen atmosphere of 500 Pa until the preset treatment temperature of 470 °C was attained. Then a reactive gas mixture of 2% CH_4+98% H_2 was introduced into the chamber and the treatment was conducted for 15 h.

Samples were ultrasonically cleaned in acetone and mounted in a holder made of polychlorotrifluoroethylene (PCTFE), at the bottom of a hole 8-mm in diameter and 5-mm deep, facing upward to facilitate removal of evolving hydrogen gas. Exposed surface area was 0.45 cm^2. The holder was inserted into a larger polytetrafluoroethylene (PTFE) cell (inner dia. 65 mm, height 100 mm) with the solution examined.

Measurements were carried out on samples:

(a) untreated (not subjected to carburization); the samples were polished with 1 μm diamond spray;

(b) carburized; they were without soot, if not otherwise indicated (carbon soot was removed by rubbing on a microcloth wetted with ethanol).

Electrochemical measurements were performed in a solution of 25 wt.% KOH at 80°C (conditions typical for industrial electrolysers for hydrogen production [5,6]). The solution was prepared from the reagent "Potassium Hydroxide semiconductor grade, 99.99% trace metals basis" made by Sigma-Aldrich. The solution was preelectrolysed using nickel electrodes at cathodic current density of 5 mA cm^{-2} for one week to prevent electrodeposition

of heavy metals, in particular of iron, during measurements [13]. Fresh solution was prepared for examination of each of the materials. Estimated value of pH at room temperature was 14.4 [21]. This corresponded to pH 13.3 at 80 °C [22].

The electrode potential was measured and presented in this paper against mercury oxide electrode Hg|HgO|25wt.% KOH which was held at room temperature (0.00 V vs. Hg|HgO|25wt.% KOH = 0.05 V vs. SHE). Counter electrode was made of Ni wire which was placed inside an open tube in another vessel connected through the solution. This minimised entry of gaseous oxygen from the anode to cathode compartment. Voltammetric measurements were carried out at the potential sweep rate of 1 mV s^{-1}.

Typically three to five measurements were performed for each experimental parameter, and arithmetic means with standard deviations (SD) (shown by vertical lines) were presented in this work. Curves in Figures are the most representative for the results obtained.

Surface analysis was performed with X-ray photoelectron spectroscopy (XPS). The measurements were carried out with Al Kα radiation at 10 kV and 10 mA. Depth profiles were obtained by Ar^+ sputtering at 3.0 kV and an ion gun current of 5 μA cm^{-2}. Binding energies in XPS spectra were assigned to species using the NIST XPS Database [23].

Spectra were recorded in the pulse counting mode, and atomic concentrations C_x were assessed using the relation:

$$C_x = (I_x/S_x)/\Sigma(I_i/S_i)$$

where I_x is the peak height of element X, and S_x is a relative elemental sensitivity factor.

Scanning electron microscopy (SEM) and energy dispersive X-ray spectroscopy (EDS) examinations were made with Nova NanoSEM 450. X-ray diffraction (XRD) was performed with Empyrean Series 2 XRD system using Cu Kα radiation (λ = 1.5418 Å).

3. Results

3.1. Characterisation of carburized samples

Fig. 1 shows carbon concentration-depth profiles determined with Glow Discharge Optical Emission Spectroscopy (GDOES) for carburized nickel: as-treated (with soot) and after rubbing (without soot). For the as-treated nickel, concentration plateaux of C and Ni to the depth of about 0.4 μm were evidently associated with soot. The decreasing C concentration at larger depths suggests the presence of carbon inside the metal. After rubbing, the profiles of C and Ni were without plateaux; they showed a regular change of concentrations with depth. The profiles indicate that carbon diffused into nickel matrix to the depth of about 0.5 μm.

Cross sections of carburized Ni and 10Ni-Fe are shown in Fig. 2. Metallographic procedure involved sectioning, then electroplating with Ni for surface protection, mounting in polymer resin and etching in the Marble reagent to reveal the microstructural features under optical microscope. Cross sections revealed the presence of surface layers in 10Ni-Fe (in this Figure it is indicated by horizontal arrow below Ni plating) and 1Ni-Fe alloys (not shown). Thickness of the layer was about 2 μm. Nickel and high-Ni alloys did not exhibit continuous layers, but on some samples traces of possible thin layers were noticed (not shown here).

X-ray diffraction (XRD) peaks (Fig. 3a) for carburized nickel can be indexed for fcc Ni with a lattice parameter of 0.352 nm which is the same as for untreated Ni. This indicates that the concentration of carbon in the metal was too small for causing a measurable lattice expansion in the depth analysed by XRD. Diffraction patterns of carburized high-Fe alloys (10Ni-Fe and 1Ni-Fe) differed from those for untreated alloys, as can be seen for untreated and carburized 10Ni-Fe (Fig. 3b). The pattern for carburized 10Ni-Fe can be ascribed to cementite (Fe_3C or $(Fe,Ni)_3C$), because indices for $(Fe_2Ni)C$ (marked by **c** at angles indicated by dots) are close to the diffracted beams. A similar diffraction pattern was also obtained for

1Ni-Fe (not shown here). Based on these data, the surface layers observed on cross sections of carburized 10Ni-Fe and 1Ni-Fe can be identified as cementite.

These results are in agreement with [19] showing the formation of Fe_3C or $(Fe,Ni)_3C$ in Fe-Ni alloys with Ni content 10 wt.% and less. Probably, traces of possible layers on high-Ni alloys (mentioned above) may also be carbides, because Fe–Ni–C phase diagram at 650 °C [24] and calculated equilibrium carbon activity for cementite formation [19] show that mixed carbides $(Fe,Ni)_3C$ are thermodynamically stable up to high nickel levels at high carbon activity.

Surface hardness (measured under indentation load of 50 g, average of 5 measurements) for untreated and carburized materials is presented in Fig. 4. The hardening effect of carburizing was the highest for 10Ni-Fe and 1Ni-Fe (increase by 35% and 23%, respectively). This demonstrates that this effect was associated mainly with the presence of carbide layers.

Surface composition was determined with XPS analysis. Fig. 5 shows profiles of concentration vs. sputtering charge for C, O and Ni on untreated and carburized Ni stored in the air for about three months. On untreated sample, the profiles changed strongly with sputtering, demonstrating a small thickness of carbon- and oxygen- containing surface film. This carbon appeared as a surface contamination (adsorbed from the air). In contrast, on carburized samples the amount of C was much higher and almost constant during the entire sputtering. After a prolonged sputtering of the surface without soot (after rubbing) there was about 0.8 at.% C. This high concentration indicates that carbon was present not only at the outer surface, but it also entered into the metal matrix. For the sample "with soot" the content of carbon was initially higher than that without soot, evidently due to carbon being deposited on the surface.

3.2. Hydrogen evolution reaction (HER)

Electrochemical measurements were carried out in the sequence:
(i) cathodic polarization at current density of 20 mA cm^{-2}, then
(ii) polarisation at -1.25 V, then
(iii) potential sweep from -1.25 V to -0.6 V at the sweep rate of 1 mV s^{-1}.
Given parameters were chosen arbitrarily: current of 20 mA cm^{-2} corresponds to hydrogen evolution at moderate rate, potential -1,25 V is close to the potential at 20 mA cm^{-2}, at potential -0.6 V there occurs anodic oxidation of Ni or Ni-Fe.

Representative curves of these measurements for untreated and carburized Ni, 90Ni-Fe and 10Ni-Fe are shown in Fig. 6. For untreated materials it was characteristic that potentials (Fig. 6(a)) initially shifted in the noble direction, passed a maximum within a few minutes, and then shifted in the negative direction. Nobler potentials indicate higher activity toward HER, therefore, this behavior indicates a short-lasting activation which was followed by deactivation. In contrast, potentials of carburized samples rather did not show a deactivation; potentials rose to nobler values than those for untreated samples, demonstrating higher activity.

The same trend was shown by cathodic currents at -1.25 V (Fig. 6(b)). Currents for carburized samples were higher as compared to untreated materials.

Similarly, polarisation curves (Fig. 6 (c)) showed higher cathodic currents for carburized materials, however, increased were also anodic currents. Anodic currents can be associated with the oxidation both of desorbing hydrogen and of cathode's metal, therefore, higher anodic currents for carburized materials might be due both to more intense hydrogen absorption and to faster corrosion.

Fig. 7 shows arithmetic means with standard deviation for: (a) potentials at 20 mA cm^{-2} after 3 h, and (b) current densities after 1 h for the materials examined. The following is observed:

(i) Activity toward HER increased with the rising content of Fe in the materials; this is in agreement with the observations reported in [10];

(ii) Carburization resulted in the improvement of activity of the materials (with the exception of 60Ni-Fe).

3.3. Surface appearance after cathodic polarisation. Examination with SEM/EDS

Surfaces of untreated and carburized 10Ni-Fe after cathodic polarisation at 20 mA cm^{-2} for 7 days are shown in Fig. 8(a) and 8(b), respectively. The surface of untreated alloy exhibits many small pits, whereas the surface of carburized alloy is much less corroded.

3.4. Surface films after cathodic polarisation. Examination with XPS

Samples were cathodically polarised at 30 mA cm^{-2} for 24 h, then washed ultrasonically in demineralised water, rinsed with ethanol and immediately placed in the XPS spectrometer. The concentration – sputtering profiles for chosen elements on untreated and carburized samples are depicted in Fig. 9. They show the following.

(i) On untreated Ni, concentration of O was higher than that in the air (Fig. 5), indicating the formation of oxide products during cathodic polarisation. Carburized surface contained mainly C; its atomic concentration (about 0.9) remained almost unchanged during sputtering.

(ii) On untreated Ni-Fe alloys, during sputtering till about 300 mA min. the rise of Fe concentration corresponded closely to the decrease of O concentration, suggesting that surface products were composed mainly of iron oxides.

(iii) Unlike in carburized Ni, in carburized Ni-Fe alloys concentration of C slightly decreased with sputtering.

(iv) In carburized materials, atomic concentration of C (0.75 to 0.95) strongly exceeded the concentration in $(Fe,Ni)_3C$. This suggests that the outermost surface of carburized materials contained mostly carbon, but not cementite $(Fe,Ni)_3C$.

3.5. Exposure under open-circuit conditions. Examination with XPS

To simulate conditions during shutdowns of electrolysers (cathodes undergo corrosion at open-circuit potential (OCP)), materials were exposed under open-circuit conditions. Fig. 10 shows OCP of untreated and carburized 10Ni-Fe as a function of immersion time. Starting from similar initial values, potential for untreated alloy shifted in the noble direction, while that for carburized alloy shifted in the negative direction. After a day, potentials for each material shifted by about 0.1 V in the noble direction. The Pourbaix diagrams at elevated temperatures for Fe [25] and Fe-Cr-Ni [26] indicate that at the attained potentials, surface film on untreated 10Ni-Fe can contain mainly $Fe(OH)_4^-$ and possibly also $NiFe_2O_4$, whereas the film on carburized 10Ni-Fe can contain mainly $Fe(OH)_4^{2-}$. The potential of carburized alloy is close to the potential for HER (it is close to the reversal potential given in [25,26] and to zero-current potentials in Fig.6), hence this potential might be associated with the hydrogen involving reaction $2H_2O \leftrightarrow H_2 + 2OH^- + 2e$. The shift of the potentials indicates that the carburization diminished the ability of the alloy for passivation.

Surface films were analysed with XPS. Samples were removed from the solution after 24-h immersion, washed ultrasonically in demineralised water, dried in the air and placed in the XPS spectrometer. The XPS concentration–sputtering profiles of the constituents and spectral

lines Fe $2p_{3/2}$ are shown in Fig. 11. Sputter charge of 5 mA min corresponds roughly to 0.1 nm Fe_2O_3. Fig. 11 indicates the following.

(i) The concentration-sputtering profiles (Fig. 11a) show that concentration of oxygen on untreated sample was higher than that on carburized sample. This indicates that the formation of oxide species on carburized sample was less intense than that on untreated one. This is in accord with the potentials attained on these materials (Fig. 10).

(ii) Binding energies (BE) in the Fe $2p_{3/2}$ line (Fig. 11b) indicate the presence of oxygen-containing iron species in the outermost surface film on untreated sample. Using the XPS Database [23], the species can be assigned to oxides and oxyhydroxides of iron (FeOOH, Fe_2O_3, Fe_3O_4, FeO) including $Fe(OH)_4^-$ which is inferred from the Pourbaix diagrams for this system. Sputtering for 60 mA min resulted in the appearance of a peak at 707 eV characteristic for metallic iron, indicating the attainment of metal substrate.

The spectra for the carburized surface did not show a maximum at BE for oxygen-containing iron species. From Fig.11a it can be inferred that the surface layer contained mainly carbon. Metallic iron in this substrate was attained after sputtering for 600 mA min (about 10 times more than that for untreated alloy).

The Ni $2p_{3/2}$ lines (not shown here) indicated the presence of oxygen-containing nickel species. This is in accord with the electrochemical equilibrium which considers the occurrence of $NiFe_2O_4$ [26]. However, it is not possible to unambiguously identify this compound, because its BE (855.4 eV [27]) is within the range of BE (855 – 856 eV) for $Ni(OH)_2$, Ni_2O_3, NiO, $Ni(OH)_2$, or NiOOH [23].

These results indicate that on carburized 10Ni-Fe alloy, unlike on untreated alloy, oxide surface products formed only in negligible amounts, suggesting high resistance of carburized material to corrosion under open-circuit conditions.

4. Discussion

Results of this work show that plasma carburizing has advantageous effect on performance of cathodes for hydrogen production. It improves the electroactivity toward HER, increases hardness and corrosion resistance. The increase in hardness and corrosion resistance by plasma carburizing is also known for stainless steel [14].

The improvement of electroactivity can be ascribed both to the increase in true surface area and to a specific catalytic effect. We suggest that plasma carburizing causes surface modification similar to metal dusting which occurs in strongly carburizing gas atmospheres at elevated temperatures (400 °C – 1000 °C) and consists in disintegration of metals and alloys (alloy steels, Ni- and Co-base alloys) into metal particles in a coke deposit [19,28,29]. The disintegration is the consequence of the volume expansion caused by graphite. In paper [19] it was shown that coke on nickel and Fe–Ni alloys consisted of graphite filaments (diameter 0.2-0.3 μm, and smaller on high Ni alloys) and particle clusters. Filaments and clusters carried metal-rich particles: metal (in Cr-Ni steels and Ni-base materials) or cementite Fe_3C (in iron and high-iron alloys).

We suggest that the surface of plasma carburized samples can be analogous to that described above, because plasma carburizing involves high carbon activity in the gas mixture and is carried out at elevated temperature (470 °C). The surface can be strongly disintegrated, and carbon filaments or clusters might be formed with metal-rich particles. The presence of metal particles in carbon can be inferred from the XPS analysis showing small amounts of Ni or Fe in carburized layers (Figs. 5,9,11). The outermost surface of carburized materials did rather not contain cementite $(Fe,Ni)_3C$ because the atomic concentration of carbon (0.75 to 0.95, Fig. 9) was much higher than that in cementite (0.25). We suppose that the graphite-

metal particles might catalyse HER similarly, as metal-rich particles were found to have catalytic effect on graphite deposition [19].

In conclusion, we suggest that the enhanced electroactivity of carburized materials toward HER is due both to the enlarged surface area and to catalytic effect of carbon-metal particles.

5. Conclusions

Untreated and plasma carburized nickel and nickel-iron alloys (with 90, 60, 10 and 1 wt.% Ni) were examined in 25% KOH at 80 °C (conditions of commercial alkaline water electrolysis for hydrogen production). Main conclusions are as follows.

1. Plasma treatment in the CH_4+H_2 gas mixture at 470 °C was effective in introducing carbon into the materials used. After a 15-h treatment, carbon entered to the depth of about 0.5 μm into nickel and formed about 2-μm thick carbide layer in high-Fe alloys.
2. Carburization resulted in an improvement of electroactivity toward HER. The improvement varied rather irregularly with the material composition; it was most significant for Ni and 1Ni-Fe.
3. Carburization also increased corrosion resistance. In consequence, amount of oxide products on carburized materials was much smaller than that on untreated ones.
4. It is suggested that plasma carburizing leads to surface changes similar to metal dusting, involving metal disintegration and formation of carbon-metal particles.
5. It is proposed that the enhanced electroactivity of carburized materials is due to the enlarged surface area and possibly to catalytic effect of carbon-metal particles.

Acknowledgement

A support by the Polish NCN through grant DEC-2012/05/B/ST5/00751 is gratefully acknowledged. Thanks are also due to Dr. A. Gajek for the SEM/EDS and XRD examinations and to M. Jaskólska for the XPS analysis.

References

[1] J. Mergel, W. Maier, D. Stolten, Hydrogen production by water electrolysis: A review of the current status and future trends, in: 20th World Hydrogen Energy Conference 2014, Gwangju, South Korea, June 15-20, 2014, paper 2217_1.pdf.
[2] J. Mergel, M. Carmo, D.L. Fritz, Status on technologies for hydrogen production by water electrolysis, in: Transition to renewable energy systems, D. Stolten, V. Scherer (Eds.), Wiley-VCH, Weinheim, 2013, pp. 425 - 450.
[3] D. Pletcher, X. Li, Prospects for alkaline zero gap water electrolysers for hydrogen production, Int. J. Hydrogen Energy 36 (2011) 15089-15104.
[4] Kai Zeng, Dongke Zhang, Recent progress in alkaline water electrolysis for hydrogen production and applications, Progress in Energy and Combustion Science 36 (2010) 307-326.
[5] S. Trasatti, Electrocatalysis of hydrogen evolution: progress in cathodic activation, in: H. Gerischer, C.W. Tobias (Eds.), Advances of Electrochemical Science and Engineering, Vol. 2, VCH, Weinheim, 1992, pp. 1-85.
[6] E. Guerrini, S. Trasatti, Electrocatalysis in water electrolysis, in: P. Barbaro, C. Bianchini (Eds.), Catalysis for Sustainable Energy Production, Wiley-VCH, Weinheim, 2009, pp. 235-269.

[7] S. Meguro, T. Sasaki, H. Katagiri, H. Habazaki, A. Kawashima, T. Sakaki, K. Asami, K. Hashimoto, Electrodeposited Ni-Fe-C cathodes for hydrogen evolution, J. Electrochem. Soc. 147 (2000) 3003-3009.
[8] M. Jafarian, O. Azizi, R. Gobal, M.G. Mahjani, Kinetics and electrocatalytic behavior of nanocrystalline CoNiFe alloy in hydrogen evolution reaction, Int. J. Hydrogen Energy 32 (2007) 1686-1693.
[9] R. Solmaz, G. Kardas, Electrochemical deposition and characterization of NiFe coatings as electrocatalytic materials for alkaline water electrolysis, Electrochim. Acta 54 (2009) 3726-3734.
[10] I. Flis-Kabulska, J. Flis, Activity of Ni-Fe cathodes toward alkaline water electrolysis and effect of anodic oxidation, submitted to Corros. Sci.
[11] N. Jiang, H.-M. Meng, L.-J. Song. H.-Y. Yu, Study on Ni-Fe-C cathode for hydrogen evolution from seawater electrolysis, Int. J. Hydrogen Energy 35 (2010) 8056-8062.
[12] L.J. Song, H.M. Meng, Effect of carbon content on Ni-Fe-C electrodes for hydrogen evolution reaction in seawater, Int. J. Hydrogen Energy 35 (2010) 10060-10066.
[13] I. Flis-Kabulska, J. Flis, Y. Sun, T. Zakroczymski, Hydrogen evolution on plasma carburized nickel and effect of iron deposition from the electrolyte in alkaline water electrolysis, Electrochim. Acta 167 (2015) 61-68.
[14] Y. Sun, Corrosion behaviour of low temperature plasma carburized 316L stainless steel in chloride containing solutions, Corros. Sci. 52 (2010) 2661-2670.
[15] H. Bala, I. Kukula, K. Giza, B. Marciniak, E. Rozycka-Sokolowska, H. Drulis, Evaluation of electrochemical hydrogenation and corrosion behaviour of $LaNi_5$-based materials using galvanostatic charge/discharge measurements, Int. J. Hydrogen Energy 37 (2012) 16817-16854.
[16] M. Singleton, P. Nash, The C-Ni (carbon-nickel) system, J. Phase Equilibria 10 (1989) 121-126.
[17] C.D.A. Brady, E.J. Rees, G.T. Burstein, Z.H. Barber, Passivation, electrocatalytic behavior of an amorphous nickel-carbon film in sulfuric acid, J. Electrochem. Soc. 155 (2008) B461–B466.
[18] G.E. Haslam, X.-Y. Chin, G.T. Burstein, X-ray photoelectron spectroscopy of the passive surface of nickel-carbon electrocatalysts after polarisation in sulfuric acid, Electrochim. Acta 118 (2014) 157-162.
[19] J. Zhang, D. J. Young, Coking and dusting of Fe–Ni alloys in $CO–H_2–H_2O$ gas mixtures, Oxid. Met. 70 (2008) 189–211.
[20] Y. Sun, X.L. Li, T. Bell, Low temperature plasma carburising of austenitic stainless steels for improved wear and corrosion resistance, Surf. Eng. 15 (1999) 49-54.
[21] I. Flis-Kabulska, J. Flis, Hydrogen evolution and corrosion products on iron cathodes in hot alkaline solution, Int. J. Hydrogen Energy 39 (2014) 3597-3605.
[22] V. Ashworth, P.J. Boden, Potential-pH diagrams at elevated temperatures, Corros. Sci. 10 (1970) 709-718.
[23] NIST X-Ray Photoelectron Spectroscopy Database. NIST Standard Reference Database 20, Version 3.0 (Data compiled and evaluated by C.D. Wagner, A.V. Naumkin, A. Kraut-Vass, J. W. Allison, C.J. Powell, J. R. Rumble Jr.), http:/srdata.nist.gov/xps.
[24] A.D. Romig Jr., J.I. Goldstein, Determination of the Fe-rich portion of the Fe-Ni-C phase diagram, Metallurgical Transactions A9 (1978) 1599-1609.
[25] B. Beverskog, I. Puigdomenech. Revised Pourbaix diagrams for iron at 25-300 °C. Corros Sci 1996;38:2121-35.
[26] B. Beverskog, I. Puigdomenech, Pourbaix diagrams for the ternary system of iron-chromium-nickel, Corrosion 55 (1999) 1077-1087.

[27] N.S. McIntyre, M.G. Cook, X-ray photoelectron studies on some oxides and hydroxides of cobalt, nickiel and copper, Anal. Chem. 47 (1975) 2208-2213.
[28] J.Q. Zhang, D.J. Young, Metal dusting – mechanisms and preventions, J. Chinese Soc. Cor. Prot. 29 (2009) 262-276.
[29] D.J. Young, J. Zhang, C. Geers, M. Schütze, Recent advances in understanding metal dusting. A review, Materials and Corrosion 62 (2011) 7-28.

Table 1. Materials and composition

Designation	Main constituents (wt.%)
Ni	99.50 Ni, 0.09 C, 0.09 Fe
90Ni-Fe	89.2 Ni, 10.6 Fe
60Ni-Fe	60.0 Ni, 39.8 Fe
10Ni-Fe	9.6 Ni, 90.2 Fe
1Ni-Fe	1.1 Ni, 98.7 Fe

Captions

Fig. 1. GDOES carbon concentration-depth profiles in carburized nickel: as-treated (with soot) and after rubbing (without soot).

Fig. 2. Cross sections of carburized Ni and 10Ni-Fe. Horizontal arrow shows a surface layer in 10Ni-Fe.

Fig. 3. X-ray diffraction patterns for: (a) carburized nickel (peaks Ni(111) and Ni(200) are at the same angles as for Ni), and (b) untreated and carburized 10Ni-Fe. Indices at **c** are for $(Fe_2Ni)C$ at angles indicated by dots.

Fig. 4. Surface hardness (at 50 g indentation load) for untreated and carburized materials.

Fig. 5. XPS concentration–sputtering profiles for C, O and Ni on untreated and carburized Ni (with and without soot) after storage in the air for about three months.

Fig. 6. (a) Potential vs. time at cathodic current density 20 mA cm^{-2}, (a) cathodic current at -1.25 V vs. time, (c) potential sweep from -1.25 V to -0.60 V at 1 mV s^{-1} for untreated and carburized Ni, 90Ni-Fe and 10Ni-Fe.

Fig. 7. (a) Potential at cathodic current 20 mA cm^{-2} after 3 h, (b) current at -1.25 V after 1 h. Bars show arithmetic means, lines show standard deviation.

Fig. 8. SEM micrographs of untreated and carburized 10Ni-Fe after cathodic polarisation at 20 mA cm^{-2} for 7 days.

Fig. 9. XPS concentration–sputtering profiles on untreated and carburized: (a) Ni, (b) 90Ni-Fe, (c) 10Ni-Fe, and (d) 1Ni-Fe after cathodic polarisation at 30 mA cm^{-2} for 24 h.

Fig. 10. Open-circuit potentials for untreated and carburized 10Ni-Fe vs. immersion time.

Fig. 11. XPS analysis of untreated and carburized 10Ni-Fe after 24-h corrosion under open-circuit conditions, (a) concentration–sputtering profiles, (b) Fe $2p_{3/2}$ lines. Vertical bars are at average electron binding energies for given species [23].

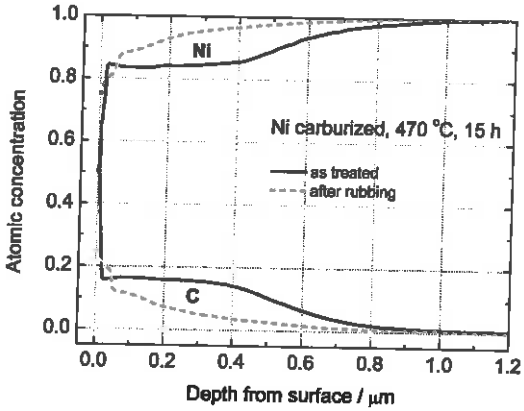
Atomic concentration
Depth from surface / μm
Ni
C
Ni carburized, 470 °C, 15 h
as treated
after rubbing
1.0
0.8
0.6
0.4
0.2
0.0
0.0
0.2
0.4
0.6
0.8
1.0
1.2

Fig. 1

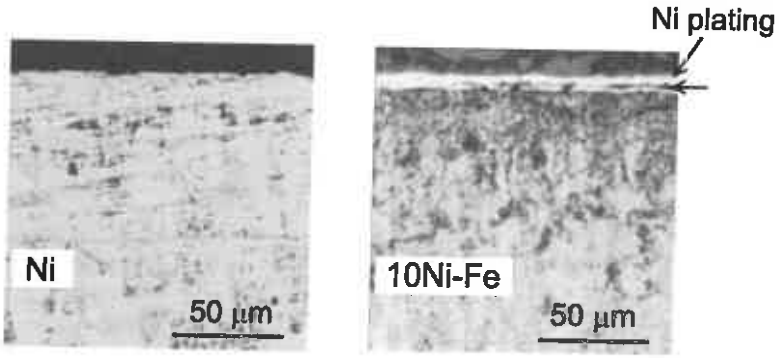
Ni plating
Ni
50 μm
10Ni-Fe
50 μm

Fig. 2

Fig. 3

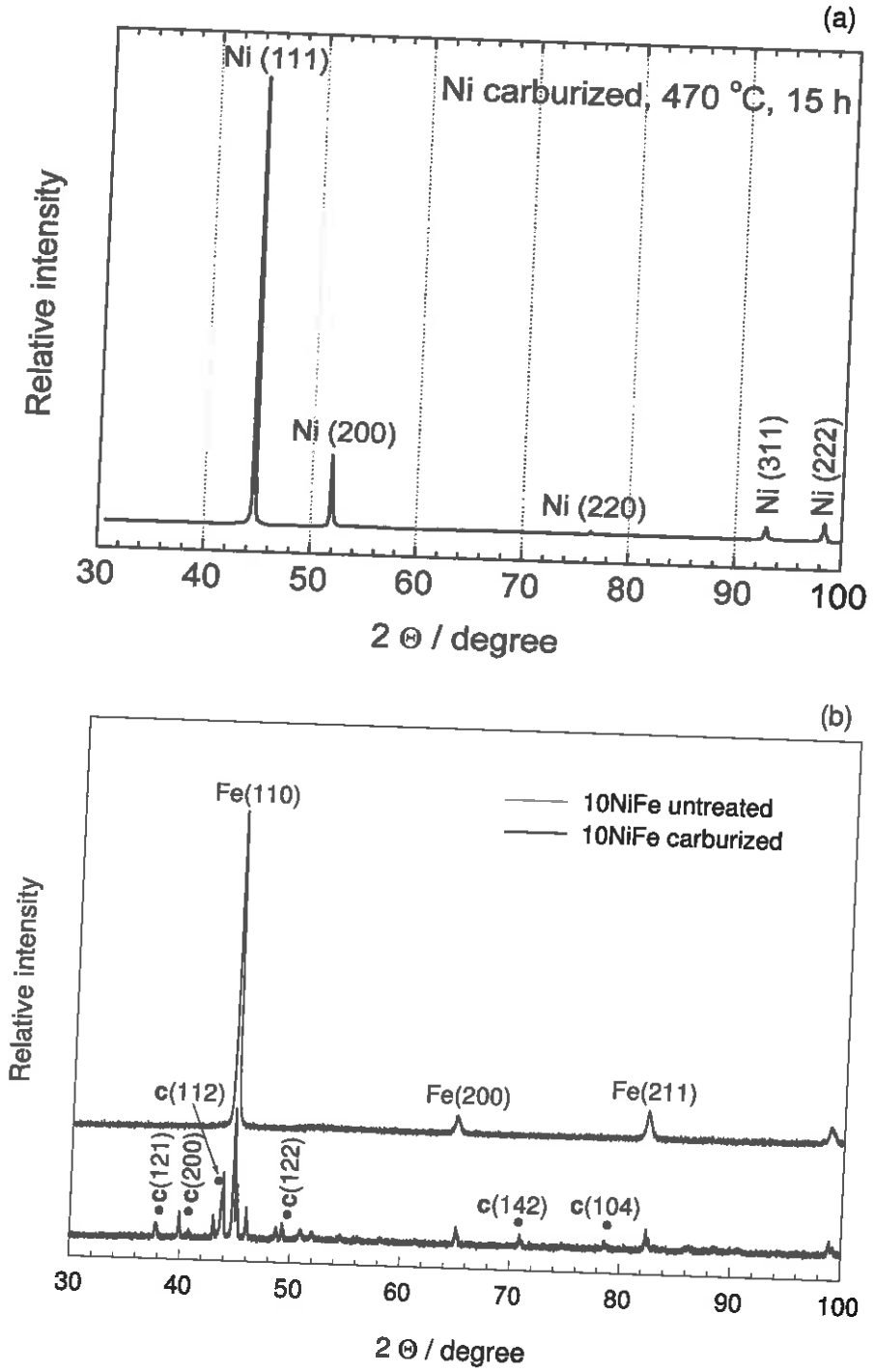
(a)
Ni carburized, 470 °C, 15 h
Ni (111)
Ni (200)
Ni (220)
Ni (311)
Ni (222)
Relative intensity
30
40
50
60
70
80
90
100
2 Θ / degree
(b)
10NiFe untreated
10NiFe carburized
Fe(110)
Fe(200)
Fe(211)
c(112)
c(121)
c(200)
c(122)
c(142)
c(104)
Relative intensity
30
40
50
60
70
80
90
100
2 Θ / degree

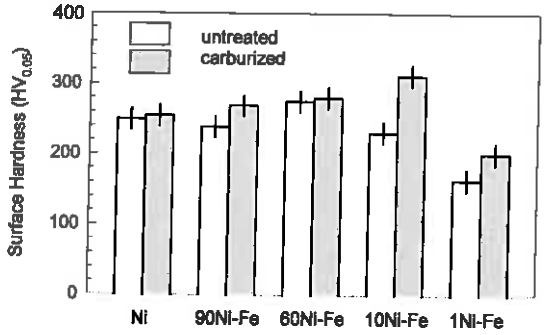

Fig. 4

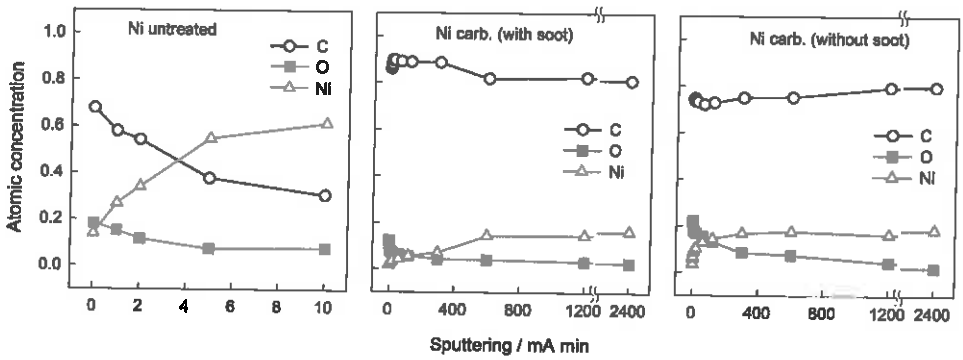

Fig. 5

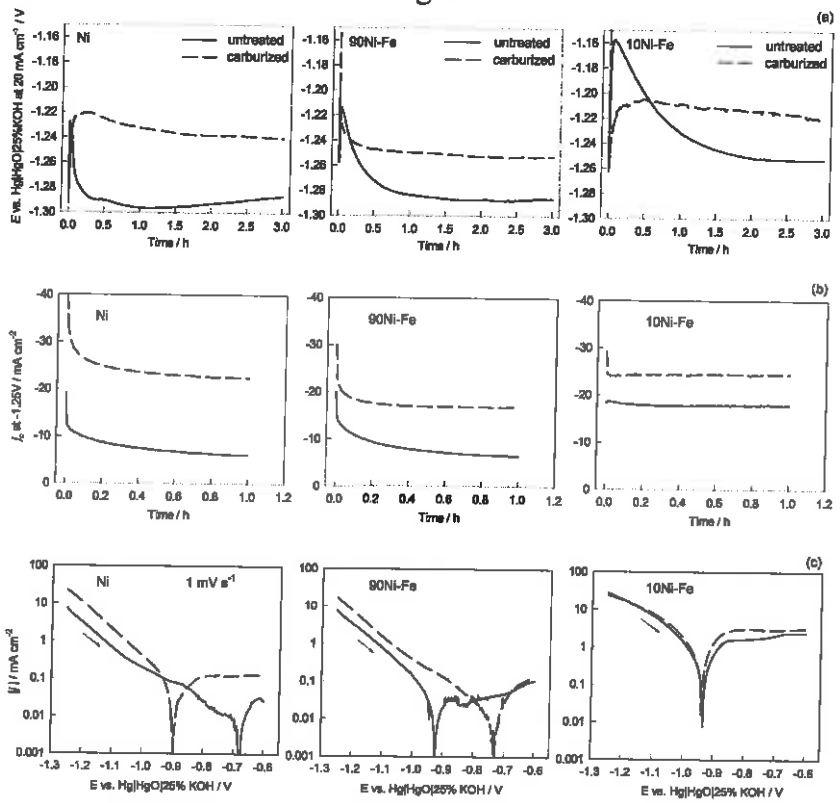

Fig. 6

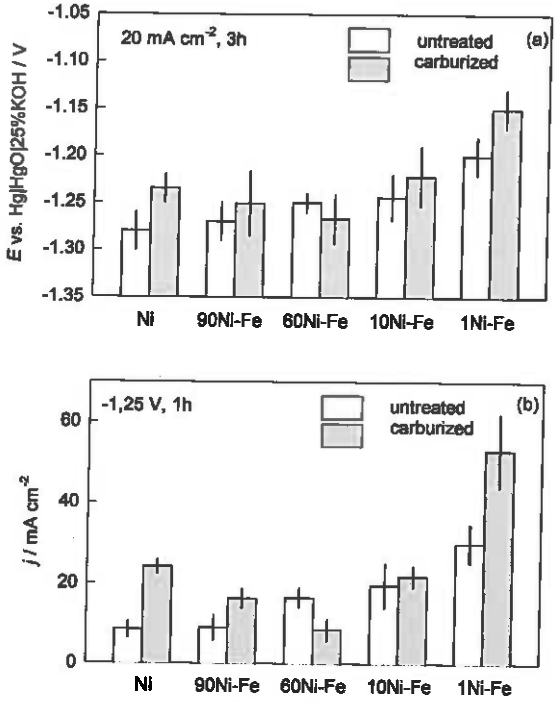

Fig. 7

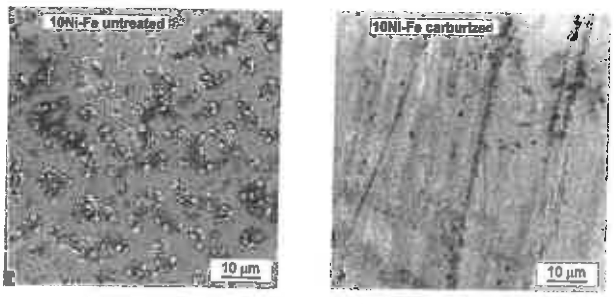

Fig. 8

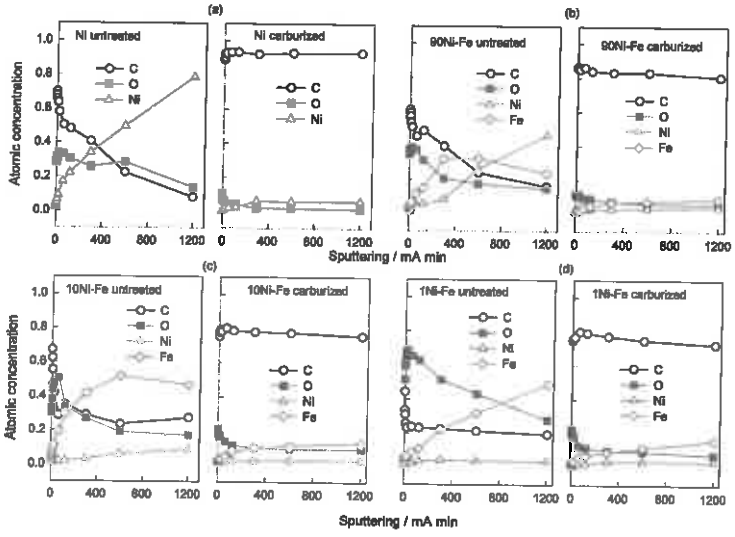

Fig. 9

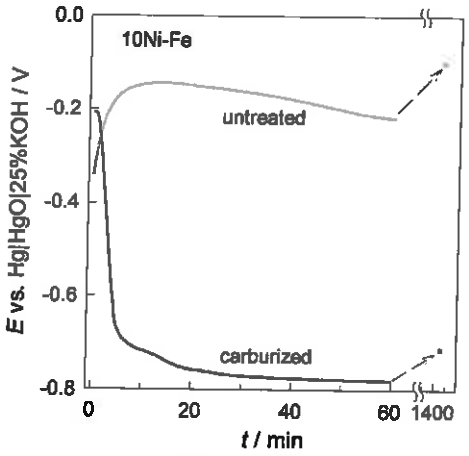
10Ni-Fe
untreated
carburized
E vs. Hg|HgO|25%KOH / V
t / min
0.0
-0.2
-0.4
-0.6
-0.8
0
20
40
60
1400

Fig. 10

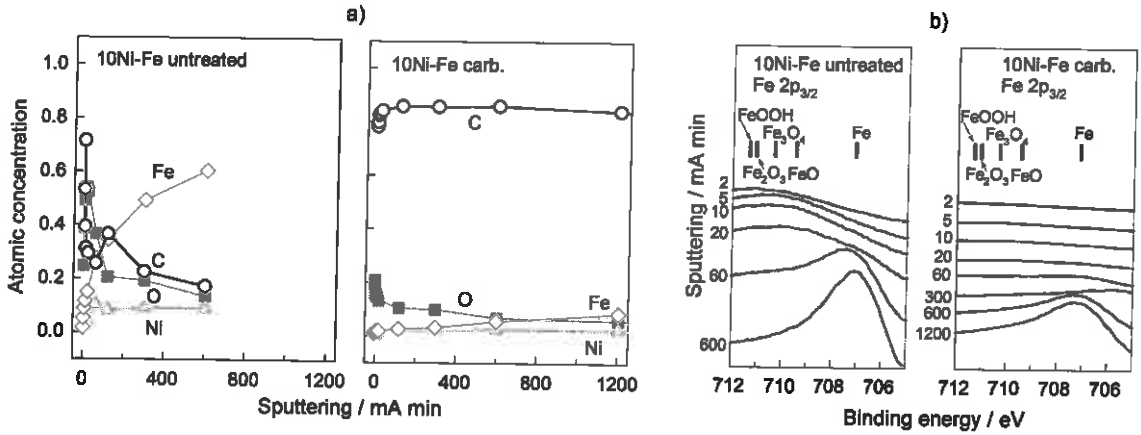
a)
b)
10Ni-Fe untreated
10Ni-Fe carb.
Atomic concentration
Sputtering / mA min
Fe
C
O
Ni
10Ni-Fe untreated
Fe 2p3/2
10Ni-Fe carb.
Fe 2p3/2
FeOOH
Fe3O4
Fe
Fe2O3FeO
Binding energy / eV

Fig. 11